Supporting Information

Ionic liquid-based electrolysis-deposition for modulating Pb crystal facet to boost CO_2 electroreduction

Chongyang Jiang,[a,b] Shaojuan Zeng,[a]* Jiaqi Feng,[c] Guilin Li,[a] Zongxu Wang,[a] Kuilin Peng,[a] Lu Bai,[a] Xiangping Zhang,[a,b]*

[a.]Beijing Key Laboratory of Ionic Liquids Clean Process, State Key Laboratory of Multiphase Complex Systems, Institute of Process Engineering, Chinese Academy of Sciences, Beijing 100190,China.

[b.]School of Future Technology, University of Chinese Academy of Sciences, Beijing 100049, China.

[c.]Key Laboratory of Colloid and Interface and Thermodynamics, Institute of Chemistry, Chinese Academy of Sciences, Beijing 100190, China.

Email: xpzhang@ipe.ac.cn, sjzeng@ipe.ac.cn

Experimental Procedures

Materials

The gas including CO_2, H_2, CO, and N_2 were purchased from Beijing Beiwen Gas Factory. Formic acid standard solution (HCOOH, HPLC grade) and phenol (C_6H_6OH, HPLC grade) were obtained from Sinopharm Chemical Regent Co., Ltd. Trifluoroacetic acid (CF_3COOH, 99.0%) was purchased from Macklin Biochemical Co., Ltd. 1-butyl-3-methylimidazole hydroxide ([Bmim][OH], 20 wt% in ethanol) and 1-butyl-3-methylimidazole hexafluorophosphate ([Bmim][PF_6], >99%), 1-butylpyridinium chloride ([BPy][Cl], >99%), tetrabutylphosphine chloride ([P_{4444}][Cl], >99%), 1-butyl-3-methylimidazolium chloride ([Bmim][Cl], >99%), 1-butyl-3-methylimidazolium acetate ([Bmim][Ac], >99%), and 1-butyl-3-methylimidazolium bistrifluoromethanesulfonate ([Bmim][NTf_2], >99%) were provided by Shanghai Chengjie Co., Ltd. Acetonitrile (AcN, HPLC grade) was purchased from Thermo Fisher Scientific Co, Ltd. All the aqueous solutions were prepared by Milli Q water (18.2 MΩ cm at 298.15 K).

Synthesis and characterization of ionic liquids

The 1-butyl-3-methylimidazolium trifluoroacetate ionic liquid ([Bmim][TFA] IL) was synthesized by [Bmim][OH] (20 wt% in ethanol) and CF_3COOH. 0.05 mol [Bmim][OH] was added into a 250 mL single round-bottom flask at 273 K, then an equimolar amount of CF_3COOH was added dropwise into the flask under magnetic stirring. The mixture solution was kept stirring at 273.15 K for 36 h until the color of the solution did not change. Subsequently, the water and ethanol were removed using rotary steaming at 333.15 K. Then the obtained ionic liquid was dried in a vacuum oven at 333.15 K for 36 h to remove trace water and ethanol. The structure of [Bmim][TFA] was investigated by nuclear magnetic resonance.

Products analysis

Gas products (CO and H_2) were analyzed by gas chromatography (GC, Agilent 7890A GC system) with a thermal conductivity detector (TCD) and a flame ionization detector (FID). Liquid product (formate) was analyzed using ^{1}HMR with phenol as the internal standard. The Faradaic efficiency of formate, CO, and H_2 were calculated following Equation (1):

$$FE = \frac{2Fn}{Q} \times 100\% \quad (1)$$

Where F is the Faraday constant (96485 C·mol^{-1}), n is the total amount of products (mol), and Q is the amount of total charge (C).

Calculation of overpotential and energy efficiency

In this work, the electrolyte of CO_2RR is 30 wt% [Bmim][PF_6]/AcN-H_2O (5wt%), and the reference electrode (Ag/Ag^+ electrode) used for the organic electrolyte. The equilibrium potential can be obtained by extrapolation zero partial current density.[1] [2] The equilibrium potential for formate is -1.68 V vs. Ag/Ag^+ in the in 30 wt% [Bmim][PF_6]/AcN-H_2O (5wt%). Then, the overpotential was the difference between the applied reaction potential and the equilibrium potential.

A cell energy efficiency (EE) of reduction CO_2 to formate was obtained by Equation (2):[3] [4]

$$EE_{formate} = \frac{FE(\%) * \Delta E^{0}_{formate}}{applied\ cell\ voltage} \quad (2)$$

Where, $EE_{formate}$ was the energy efficiency for the conversion of CO_2 into foramte. $\Delta E^{0}_{formate}$ was the different between the standard reaction potentials for water oxidation and the reduction of CO_2 into formate. Applied cell voltage was the difference between the water oxidation potential and the working potential at the cathode.

During the energy efficiency calculation, the applied potentials of the cathode versus Ag/Ag^+ can be transformed to the reversible hydrogen electrode (RHE), according to Equation (3).

$$E_{(Ag/Ag+)} = E_{(RHE)} - 0.54\ V - pH*0.059 \quad (3)$$

Therefore, 1 M LiCl/ethanol as the outer bridge electrolytes of InLab Science Pro-ISM electrode was used to determine the pH values in 30 wt% [Bmim][PF_6]/AcN/ H_2O (5 wt%). To ensure the accuracy of the experimental results, pH tests were repeated at least five times, and the pH of 30 wt% [Bmim][PF_6]/AcN/ H_2O (5 wt%) is 5.84, 5.82, 5.79, 5.80, 5.86. Therefore, the potential applied at the cathode can be converted into an RHE. We can calculate the EE according to Equation (2).

Density functional theory calculation details

To understand the effects of crystal facet on the performance of CO_2 electroreduction, Pb(111) and Pb(200) crystal facets were selected as the calculation model species in this study. Surface energies of Pb electrode calculated using DFT (obtained from the Crystalium, http://crystalium.materialsvirtuallab.org/). The DFT calculations were performed using the Vienna ab initio simulation package (VASP). The Perdew-Burke-Ernzerhof (PBE) of electron-exchange correlation functional on the level of generalized gradient approximation (GGA) was used for these calculations. Specifically, the van der Waals correction was employed by using Grimme DFT-D method to describe the long-range electrostatic interactions.

The Gibbs free energy (ΔG) was calculated by the following Equation (4):

$$\Delta G = \Delta E + \Delta E_{zpe} - T\Delta S \quad (4)$$

Where ΔE, ΔE_{zpe}, and ΔS are the DFT energy, zero-point energy (ZPE), and entropy of calculated species. T was set at 298.15 K in this work.

Supplementary Figures

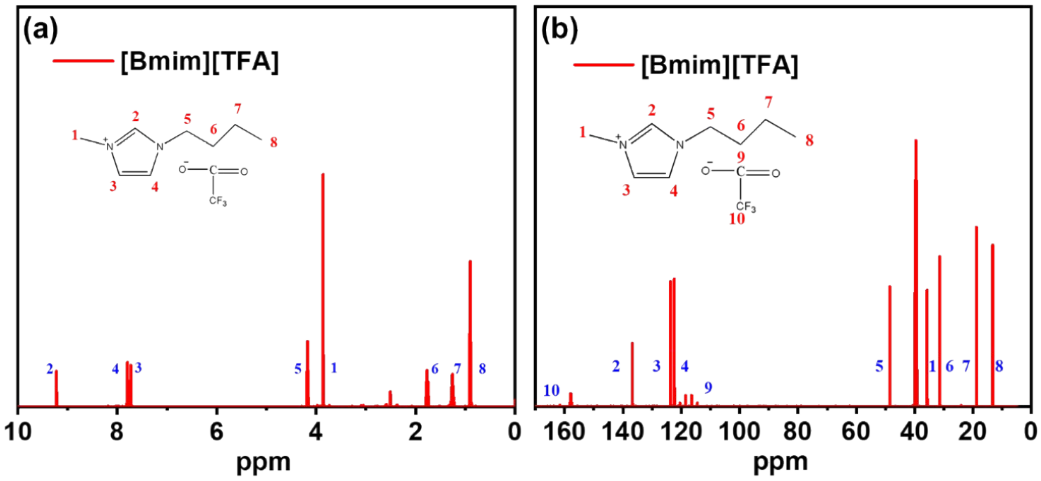

^{1}H NMR (600M Hz, DMSO-d_6): 0.90 (t, 3H.C8), 1.27 (M, 2H.C7), 1.77 (t, 2H.C6), 3.86 (s, 3H.C1), 4.17 (t, 2H.C5), 7.73 (d, 1H.C3), 7.80 (d, 1H.C4), 9.22 (s, 1H.C2)

^{13}C NMR (600M Hz, DMSO-d_6): 13.67 (C8), 19.21 (C7), 31.82 (C6), 36.13 (C1), 48.93 (C5), 114.88-120.86 (C9), 122.75 (C4), 124.08 (C3), 137.13 (C2), 158.02-158.63 (C10)

Fig. S1 (a) ^{1}H NMR and (b) ^{13}C NMR spectrum of [Bmim][TFA].

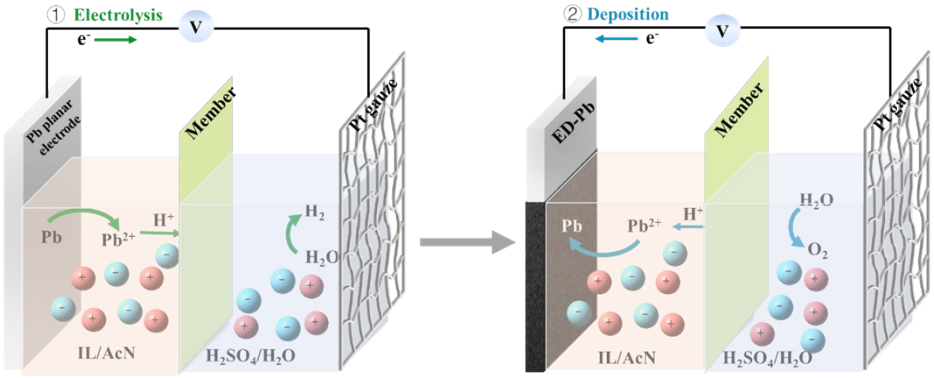

Fig. S2 Schematic illustration of the electrolysis-deposition preparation of the ED-Pb electrodes.

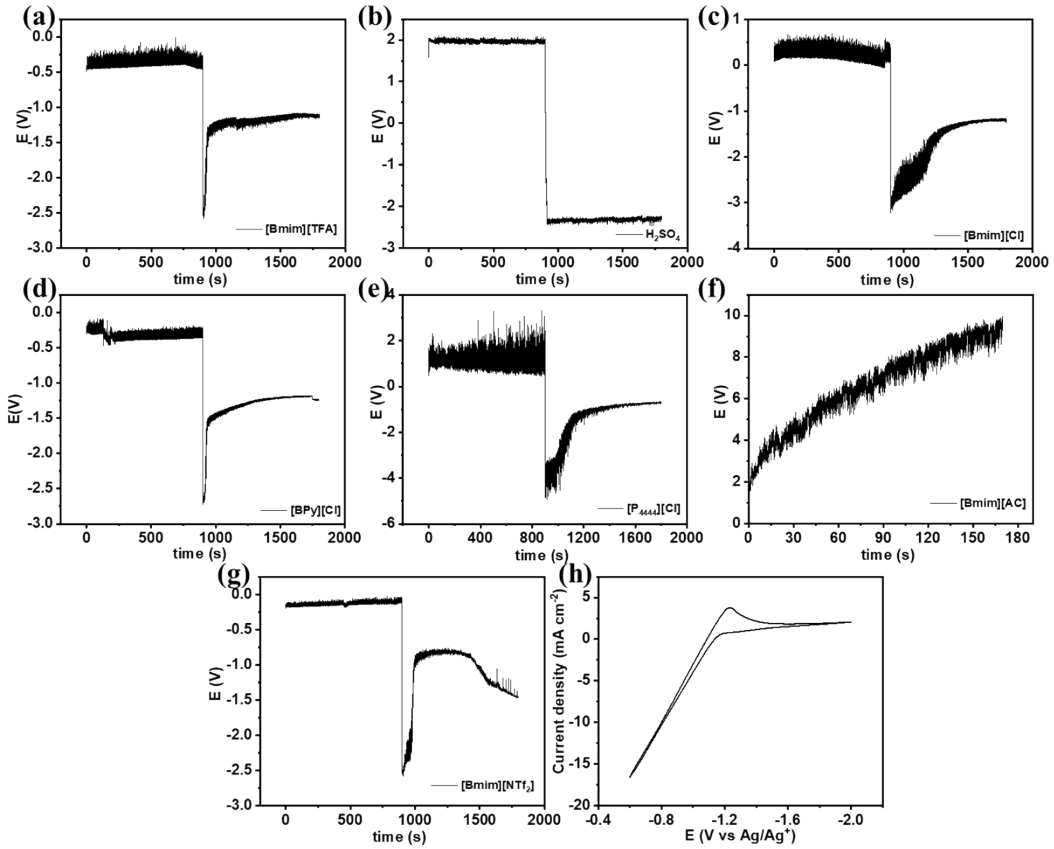

Fig. S3 The potential curves over time in (a) [Bmim][TFA], (b) H_2SO_4, (c) [Bmim][Cl], (d) [BPy][Cl], (e) $[P_{4444}][Cl]$, (f) [Bmim][AC], and (g) $[Bmim][NTf_2]$. (h) The cyclic voltammograms of $Pb(CH_3COO)_2$ in 0.5 M [Bmim][AC]/AcN electrolyte at a scan rate of 40 mV/s.

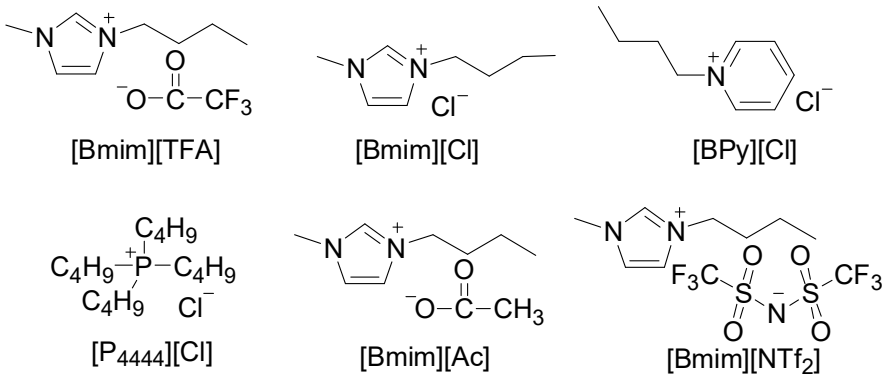

Fig. S4 Th structure of the ILs used in this work.

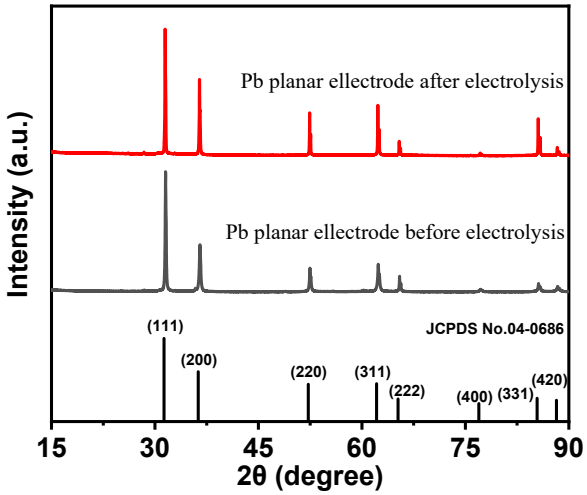

Fig. S5 XRD pattern of Pb standard PDF card (No. 04-0686) and Pb planar electrode before and after electrolysis.

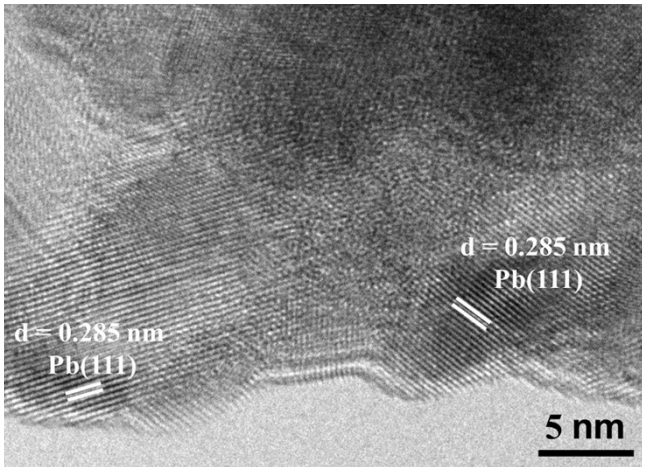

Fig. S6 TEM images of ED-Pb catalyst.

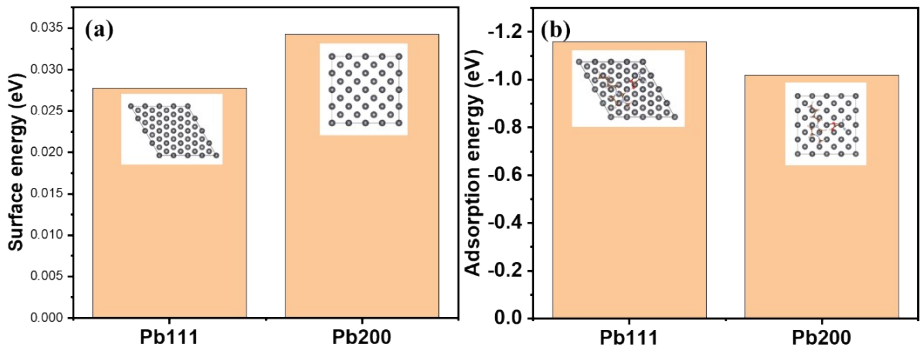

Fig. S7 (a) The surface energies and (b) adsorption energy of [Bmim][TFA] on Pb(111) and Pb(200) crystal facet.

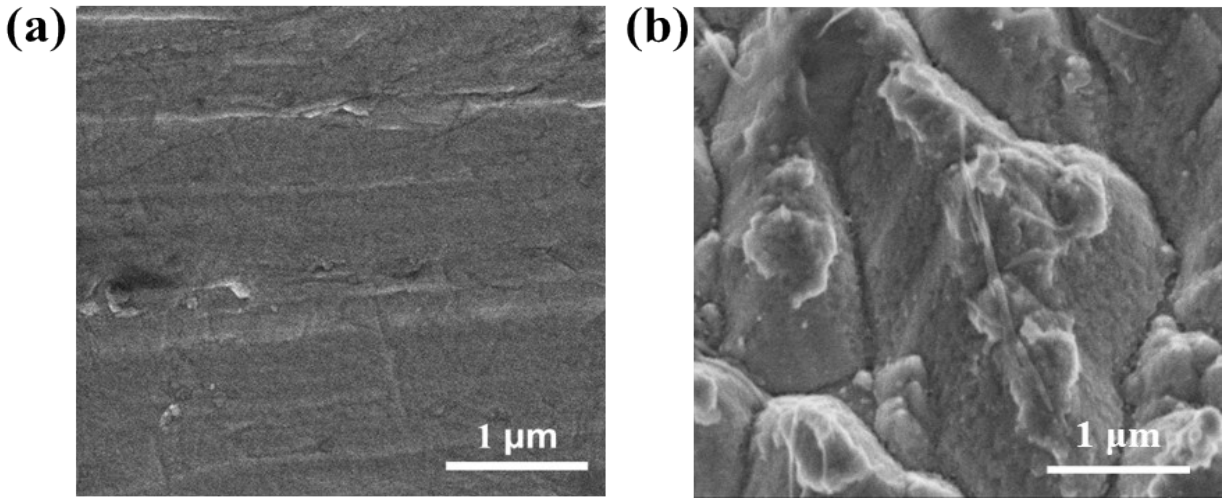

Fig. S8 SEM images of Pb planar electrode (a) before electrolysis and (b) Pb planar electrode after electrolysis.

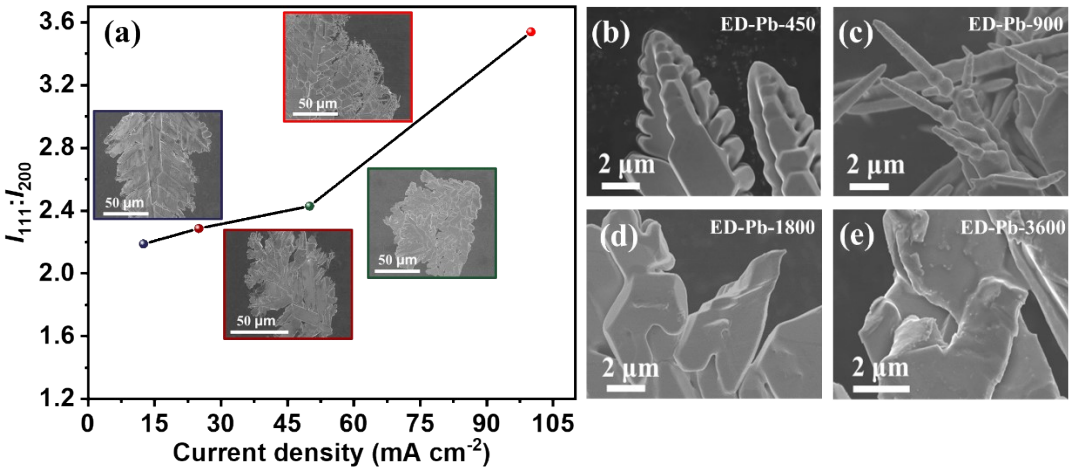

Fig. S9 (a) Peak intensity ratio of Pb(111): Pb(200) deduced from the XRD patterns. The insets in (a) show SEM images of the ED-Pb electrodes deposited at 100 mA (red), 50 mA (green), 25 mA (deep red), and 12.5 mA (blue), (b-e) SEM images of ED-Pb electrodes from ED-Pb-450 to ED-Pb-3600.

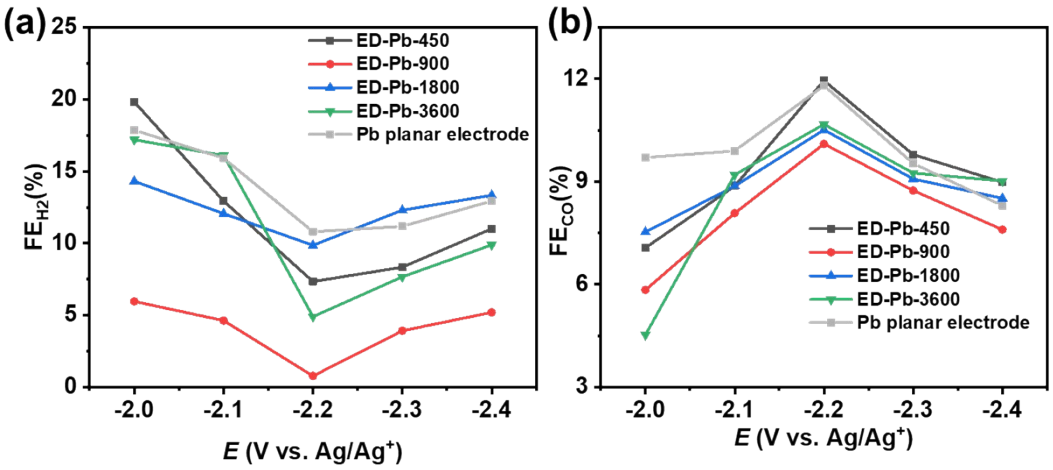

Fig. S10 FE of (a) H_2 and (b) CO on the ED-Pb electrodes and Pb planar electrode at different applied potential in CO_2-saturated [Bmim][PF_6]/AcN-H_2O electrolyte.

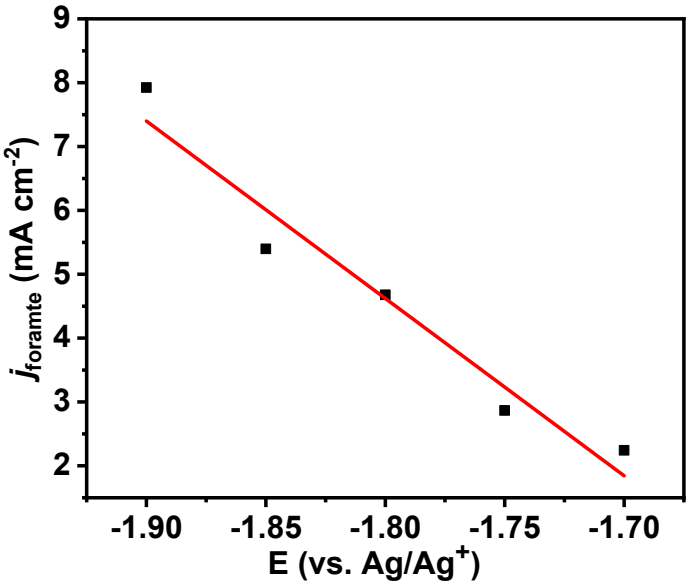

Fig. S11 Partial current density of formate under different applied potentials. The equilibrium potential can be obtained by extrapolation zero partial formate current density.

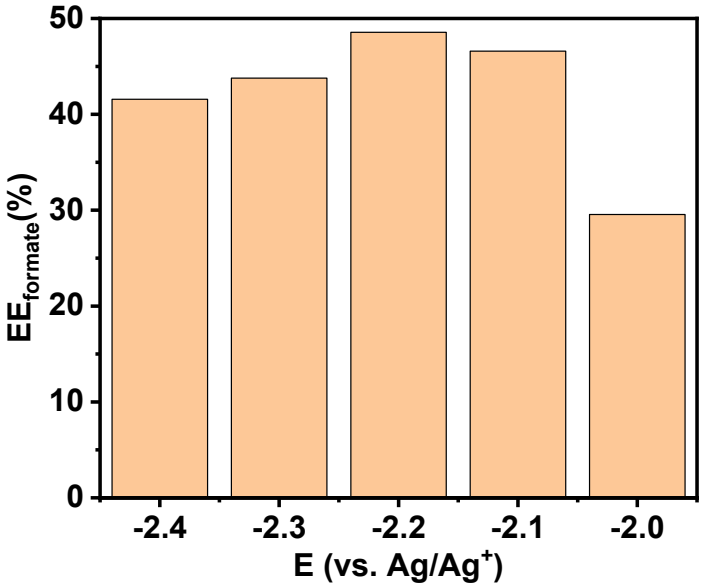

Fig. S12 The dependence of EE for CO_2 electroreduction to formate on applied voltage

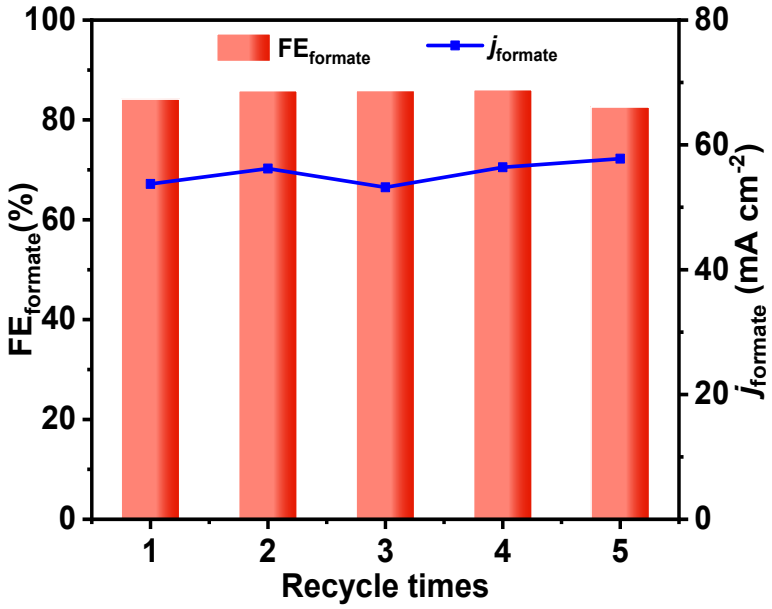

Fig. S13 Stability test for ED-Pb-900 electrode at -2.2 V in CO_2 saturated 30 wt% [Bmim][PF_6]/AcN-H_2O (5 wt%) electrolyte.

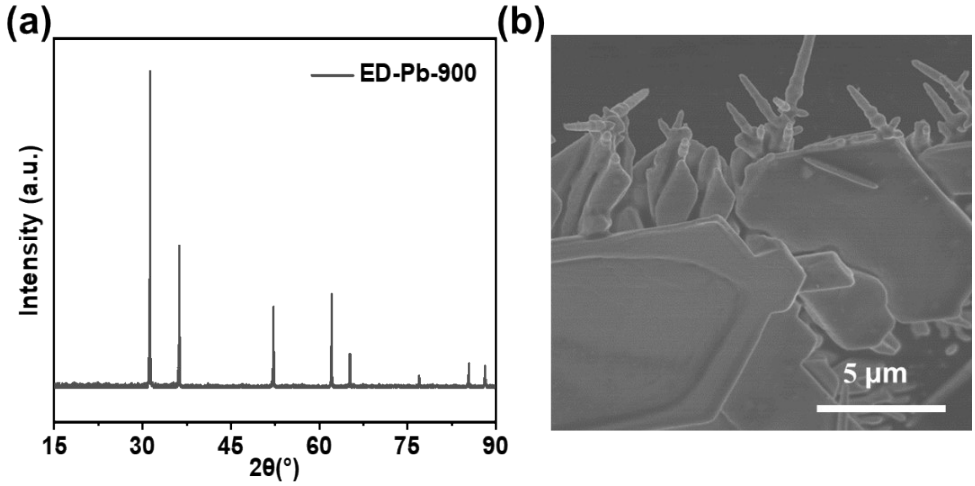

Fig. S14 (a) XRD pattern and (b) SEM image of the ED-Pb-900 after 5 h electrolysis at -2.2 V.

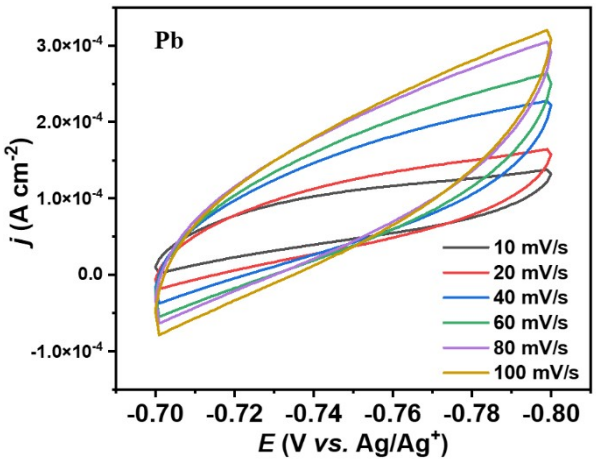

Fig. S15 Cyclic voltammograms at the range of -0.7 to -0.8 V with different scan rates for Pb planar electrode.

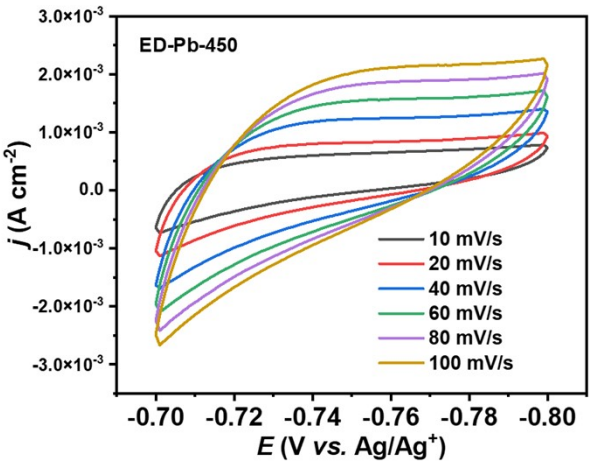

Fig. S16 Cyclic voltammograms at the range of -0.7 to -0.8 V with different scan rates for ED-Pb-450.

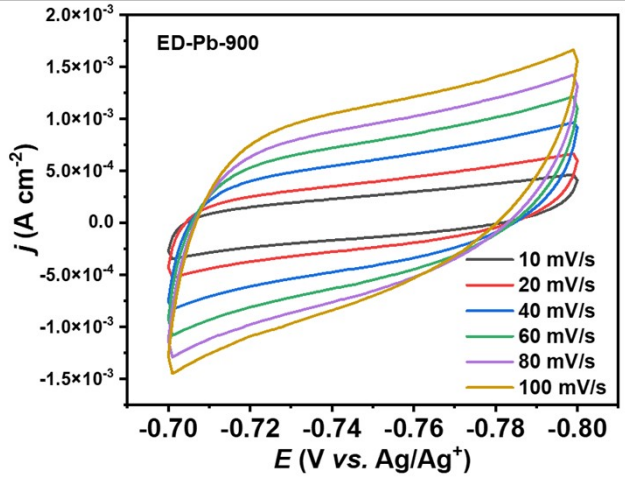

Fig. S17 Cyclic voltammograms at the range of -0.7 to -0.8 V with different scan rates for ED-Pb-900.

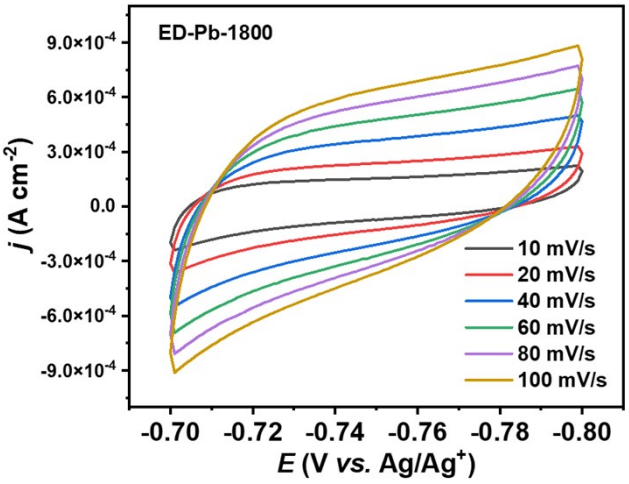

Fig. S18 Cyclic voltammograms at the range of -0.7 to -0.8 V with different scan rates for ED-Pb-1800.

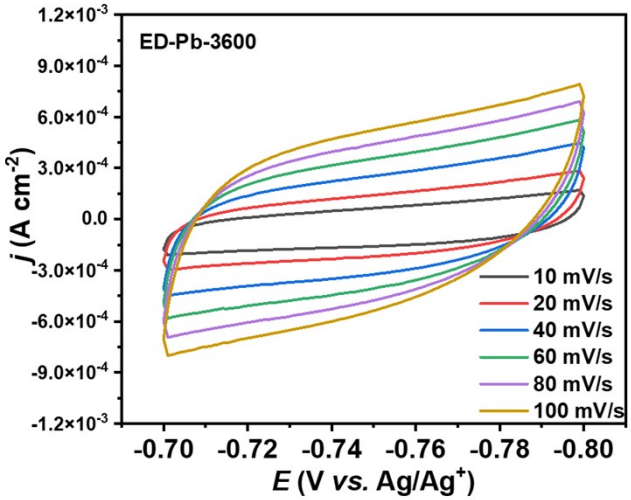

Fig. S19 Cyclic voltammograms at the range of -0.7 to -0.8 V with different scan rates for ED-Pb-3600.

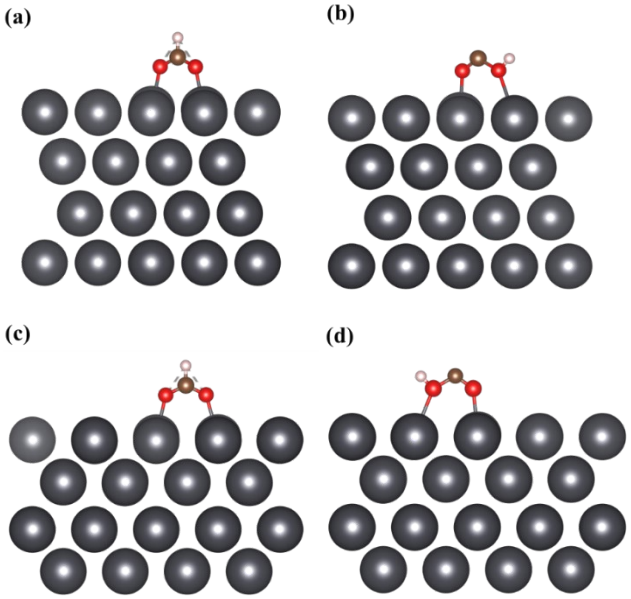

Fig. S20 Optimized configurations of (a) *OCHO and (b) *COOH on Pb(111) crystal facet. Optimized configurations of (c) *OCHO and (d) *COOH on Pb(200) crystal facet.

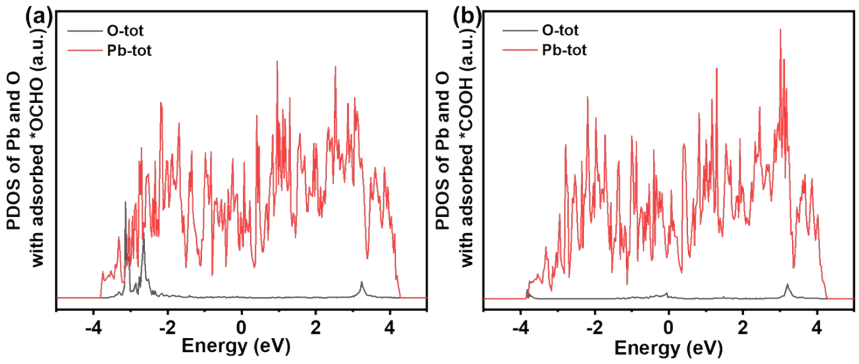

Fig. S21 PDOS of the O atom in adsorption (a) *OCHO and (b) *COOH in Pb(111) crystal facet.

Table S1. Current density and FE of formate in CO_2 electroreduction using various electrodes and catholytes.

Catalysts	Electrolyte	Overpotential (V)	$FE_{formate}$	$j_{formate}$	Ref.
Anodic polarization Pb	0.1 M $KHCO_3$	0.85	48	0.73	[5]
Pb/Cu	0.1 M $KHCO_3$	0.89	74.2	-	[6]
$Sn_{56.3}Pb_{43.7}$	0.5 M $KHCO_3$	-2.0 vs Ag/AgCl	79.8	45.2	[7]
Sulfide-derived-Pb	0.1 M $KHCO_3$	0.83	88	12	[8]
Oxide-derived Pb	0.5 M $NaHCO_3$	0.55	98	0.6	[9]
Electrochemically roughened Pb	0.1 M $KHCO_3$	0.71	88	1.17	[10]
Porous Pb(100)	1 M $KHCO_3$	0.74	97	8.0	[11]
Amine-derived Pb	1 M $KHCO_3$	0.84	80	24	[12]
Pb	[Bmim][124Triz] (700 mM)/AcN-H_2O (5 wt%)	-2.2 vs Ag/Ag^+	95.2	25.4	[13]
Octahedral Pb	0.1 M $KHCO_3$	0.65	98.2	~2	[14]
PbO_2	[Bzmim][BF_4] (14.7 wt%)/AcN-H_2O (11.7 wt%)	-2.3 vs Ag/Ag^+	95.5	40.8	[15]
SnPb alloy	[Emim][OTf]/AcN-H_2O (81:14:5)	-1.95 vs Ag/AgCl	94	7.7	[16]
Nanolayered Pb electrode	0.1 M $KHCO_3$	0.75	94.1	-	[17]
Pb	KOH/methanol	-2.0 vs Ag/AgCl	66	-	[18]
Pb granule electrode	0.2 M K_2CO_3	0.722	94	-	[19]
Pd doped $Pb_3(CO_3)_2(OH)_2$	0.1 M $KHCO_3$	0.95	90	13	[20]
Pb	[Bmim][PF_6] (30 wt%)/AcN-H_2O (5 wt%)	0.52 (-2.2 vs Ag/Ag^+)	76.7	7.45	This Work
		0.72 (-2.4 vs Ag/Ag^+)	72.3	28.38	
ED-Pb-900	[Bmim][PF_6] (30 wt%)/AcN-H_2O (5 wt%)	0.52 (-2.2 vs Ag/Ag^+)	86.4	56.4	
		0.72 (-2.4 vs Ag/Ag^+)	80.0	110.83	

Table S2. The basic parameters of the intermediates (*OCHO and *COOH) on different Pb crystal facets.

Crystal facet		Pb(111)	Pb(200)
*^{1}OCHO^{2}	^{1}O-Pb (Å)	2.47	2.48
	^{2}O-Pb (Å)	2.48	2.51
	^{1}O-C (Å)	1.27	1.27
	^{2}O-C (Å)	1.27	1.27
	H-C (Å)	1.11	1.11
	^{1}O=C=O^{2} (°)	129.10	128.74
	^{1}O=C-H (°)	115.34	115.81
	^{2}O=C-H (°)	115.55	115.45
*CO^{1}O^{2}H	^{1}O-Pb (Å)	2.57	2.61
	^{2}O-Pb (Å)	2.91	2.91
	^{1}O=C (Å)	1.23	1.23
	^{2}O-C (Å)	1.42	1.41
	H-O^{2} (Å)	0.98	0.98
	^{1}O=C-O^{2} (°)	114.31	114.73
	C-O^{2}-H (°)	105.53	105.75

Notes and References

1. D. X. Yang, Q. G. Zhu, C. J. Chen, H. Z. Liu, Z. M. Liu, Z. J. Zhao, X. Y. Zhang, S. J. Liu and B. X. Han, *Nat. Commun.*, 2019, **10**, 677.
2. J. Feng, H. Gao, L. Zheng, Z. Chen, S. Zeng, C. Jiang, H. Dong, L. Liu, S. Zhang and X. Zhang, *Nat. Commun.*, 2020, **11**, 4341.
3. C. Chen, X. Yan, R. Wu, Y. Wu, Q. Zhu, M. Hou, Z. Zhang, H. Fan, J. Ma, Y. Huang, J. Ma, X. Sun, L. Lin, S. Liu and B. Han, *Chem Sci*, 2021, **12**, 11914-11920.
4. W. Guo, S. Liu, X. Tan, R. Wu, X. Yan, C. Chen, Q. Zhu, L. Zheng, J. Ma, J. Zhang, Y. Huang, X. Sun and B. Han, *Angew. Chem. Int. Ed. Engl.*, 2021, **60**, 21979-21987.
5. M. J. W. Blom, V. Smulders, W. P. M. van Swaaij, S. R. A. Kersten and G. Mul, *Appl. Catal., B-Environ*, 2020, **268**, 118420.
6. C. Kim, T. Möller, J. Schmidt, A. Thomas and P. Strasser, *ACS Catal.*, 2018, **9**, 1482-1488.
7. S. Y. Choi, S. K. Jeong, H. J. Kim, I.-H. Baek and K. T. Park, *Acs Sustain. Chem. Eng.*, 2016, **4**, 1311-1318.
8. J. E. Pander, J. W. J. Lum and B. S. Yeo, *J. Phys. Chem. A*, 2019, **7**, 4093-4101.
9. C. H. Lee and M. W. Kanan, *ACS Catal.*, 2015, **5**, 465-469.
10. Z. He, J. Shen, Z. Ni, J. Tang, S. Song, J. Chen and L. Zhao, *Catal. Commun.*, 2015, **72**, 38-42.
11. M. Fan, S. Garbarino, G. A. Botton, A. C. Tavares and D. Guay, *J. Mater. Chem. A*, 2017, **5**, 20747-20756.
12. N. Zouaoui, B. D. Ossonon, M. Fan, D. Mayilukila, S. Garbarino, G. de Silveira, G. A. Botton, D. Guay and A. C. Tavares, *J. Phys. Chem. A*, 2019, **7**, 11272-11281.
13. J. Feng, S. Zeng, H. Liu, J. Feng and H. Gao, *ChemSusChem*, 2018, **11**, 3191-3197.
14. W. Yu, L. Wen, J. Gao, S. Chen, Z. He, D. Wang, Y. Shen and S. Song, *Chem. Commun.*, 2021, **57**, 7418-7421.
15. H. R. Wu, J. L. Song, C. Xie, Y. Hu and B. Han, *Green Chemistry*, 2018, **20**, 1765-1769.

16. A. Hailu, A. A. Tamijani, S. E. Mason and S. K. Shaw, *Energy & Fuels*, 2020, **34**, 3467-3476.
17. Y. Kwon and J. Lee, *Electrocatalysis*, 2010, **1**, 108-115.
18. SatoshiKaneco, RyosukeIwao, KenjiIiba, KiyohisaOhta and TakayukiMizuno, *Energy*, 1998, **23**, 1107-1112.
19. F. Köleli and D. Balun, *Applied Catalysis A: General*, 2004, **274**, 237-242.
20. W. Huang, Y. Wang, J. Liu, Y. Wang, D. Liu, J. Dong, N. Jia, L. Yang, C. Liu, Z. Liu, B. Liu and Q. Yan, *Small*, 2022, **18**, e2107885.